Large Motion Control of an Experimental Mobile Manipula with Limited Sensing

Norbert A.M. Hootsmans
Automation Engineering Department
Production Engineering Research Laboratory, Hitachi, Ltd.
292 Yoshida-cho, Totsuka-ku
Yokohama 244, Japan

Steven Dubowsky
Patrick Z. Mo
Department of Mechanical Engineering
Massachusetts Institute of Technology
Cambridge, MA 02139 USA

ABSTRACT

Two recently developed motion control algorithms for mobile manipulators are applied to an experimental system. The manipulator motions induce significant dynamic interactions with its vehicle and suspension. A conventional fixed-base controller, which typically neglects these dynamic interactions, is shown to lead to poor performance. Both mobile manipulator control algorithms, however, which account for dynamic vehicle motions caused by manipulator motions, are shown to perform well, despite practical limitations imposed on the sensory data available for control in field environments.

I. INTRODUCTION

Robotic and tele-robotic manipulators mounted on mobile vehicles are being considered for a wide variety of applications, such as remote fire-fighting, toxic waste cleanup, nuclear facility maintenance, and planetary exploration, see Figure 1 [1]. Unlike conventional rigid-base industrial manipulators, the motions of such a *mobile manipulator* will interact dynamically with its vehicle and suspension, causing excessive end-effector errors and poor system stability. Furthermore, highly variable system characteristics exacerbate the control problem, and unstructured and possibly hostile environments limit the sensing techniques practically applicable for control.

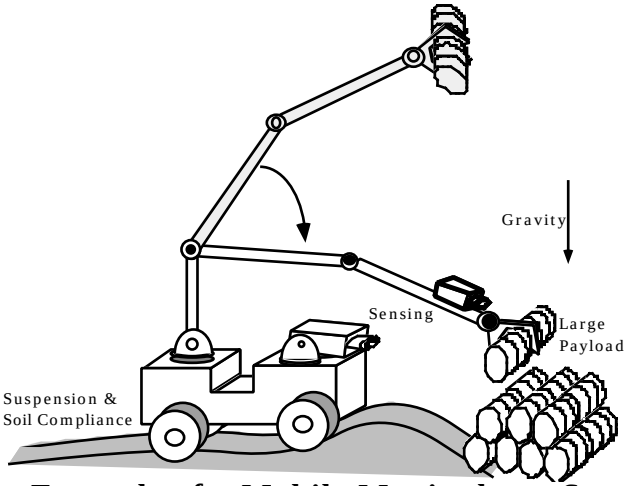

Fig. 1. Example of a Mobile Manipulator System.

Many position control approaches have been applied to fixed-base manipulators [2]. However, little research has focused on the important control problems of terrestrial mobile manipulators. Some studies simulated the system dynamics, but did not address the problem of achieving inertial endpoint motion control [3-5]. Others treated simplified forms of the problem by assuming a massive vehicle or outriggers [6,7]. Fast endpoint feedback has been used to control flexible manipulators and micro-manipulators [8,9]. This approach was applied successfully in a mobile manipulator control experiment limited to small motions near a target where endpoint sensing is feasible [10]. In practice, however, such endpoint sensing will be difficult along the entire six degree-of-freedom (DOF) trajectory of large motions in field environments. Recently, two control algorithms, the Mobile Manipulator Jacobian Transpose (MMJT) algorithm and the Mobile Manipulator Resolved Rate (MMRR) algorithm, were developed which do not rely on endpoint sensing, but instead use practically available vehicle motion sensors [11,12]. These algorithms were shown to perform well *in simulation*. This paper reports on an *experimental* study which compares the performance of the two algorithms and considers their practical utility, including such factors as computational and sensor requirements and robustness with respect to unmodelled system characteristics.

II. MOBILE MANIPULATOR CONTROL ALGORITHMS

In this section a Mobile Manipulator Jacobian (MMJ) is presented along with two mobile manipulator control algorithms derived based on the MMJ.

a. The Mobile Manipulator Jacobian

A mobile manipulator on a suspended vehicle has a non-square jacobian, similar to those found for redundant manipulators. However, the extra degrees of freedom due to the vehicle do not have control actuators, and hence one cannot simply resolve the redundancy. Instead, the MMJ was developed, which can be partitioned into two sub-jacobians, $\mathbf{J}_v$ and $\mathbf{J}_m$, where $\mathbf{J}_v$ multiplies the vehicle velocities corresponding to the uncontrolled degrees of freedom, and $\mathbf{J}_m$ multiplies the manipulator joint velocities corresponding to the controlled degrees of freedom, as shown in Equation (1) [12].

For an n DOF mobile manipulator on a 6 DOF vehicle:

$$\dot{\mathbf{x}}_e = \begin{bmatrix} \dot{\mathbf{r}}_e \\ \omega_e \end{bmatrix} = \mathbf{MMJ}\,\dot{\mathbf{q}} = [\,\mathbf{J}_v \,|\, \mathbf{J}_m\,] \begin{bmatrix} \dot{\mathbf{x}}_v \\ \dot{\mathbf{q}}_m \end{bmatrix} \qquad (1)$$

where $\dot{\mathbf{x}}_e$ is the 6 element column vector of end-effector linear and angular velocities, and where $\dot{\mathbf{r}}_e$ is the linear end-effector velocity and ω_e is the angular. The vector $\mathbf{q} = [\mathbf{r}_v^T, \theta_v^T, \mathbf{q}_m^T]^T = [x, y, z, \psi_x, \psi_y, \psi_z, \theta_1, \ldots, \theta_n]^T$ is the 6+n element position column, which includes the vehicle position, $\mathbf{r}_v$, and roll-pitch-yaw orientation, θ_v, as well as the manipulator joint displacements, $\mathbf{q}_m$. $\dot{\mathbf{q}}_m$ is the vector of n manipulator joint velocities, and $\dot{\mathbf{x}}_v$ equals $[\dot{\mathbf{r}}_v^T, \omega_v^T]^T$, where $\dot{\mathbf{r}}_v$ is the vehicle linear velocity vector and ω_v is the angular. The MMJ sub-matrices $\mathbf{J}_v$ and $\mathbf{J}_m$ were derived as [12]:

$$\mathbf{J}_v(\theta_v, \mathbf{q}_m) = \begin{bmatrix} \mathbf{I} & -\mathbf{R}_v(\theta_v)\,[{}^V\mathbf{r}_e^V(\mathbf{q}_m)]^\times\,\mathbf{R}_v^T(\theta_v) \\ \mathbf{0} & \mathbf{I} \end{bmatrix} \qquad (2)$$

$$\mathbf{J}_m(\theta_v, \mathbf{q}_m) = \begin{bmatrix} \mathbf{R}_v(\theta_v) & \mathbf{0} \\ \mathbf{0} & \mathbf{R}_v(\theta_v) \end{bmatrix} \mathbf{J}_{fbm}(\mathbf{q}_m) \qquad (3)$$

The matrix $\mathbf{J}_{fbm}(\mathbf{q}_m)$ is the conventional 6 by n jacobian of an n DOF fixed-base manipulator. $\mathbf{I}$ is the 3 by 3 identity matrix and $\mathbf{R}_v(\theta_v)$ is the 3 by 3 vehicle rotation matrix, dependent only on the vehicle orientation, which relates the vehicle frame to the inertial frame. The term ${}^V\mathbf{r}_e^V(\mathbf{q}_m)$ is the 3 element position vector of the manipulator end-effector with respect to the vehicle frame expressed in vehicle frame coordinates. $[\mathbf{a}]^\times$ is the cross product matrix for the vector $\mathbf{a}$, defined as:

$$[\mathbf{a}]^\times = \begin{bmatrix} 0 & -a_z & a_y \\ a_z & 0 & -a_x \\ -a_y & a_x & 0 \end{bmatrix} \qquad (4)$$

b. Mobile Manipulator Jacobian Transpose Control

The MMJT algorithm gives the manipulator joint torques, τ_m, for an n DOF manipulator mounted on a 6 DOF passive suspension vehicle as [11,12]:

$$\tau_m = \tilde{\mathbf{J}}_m^T(\tilde{\theta}_v, \mathbf{q}_m)\,\tilde{\mathbf{F}}_{edes} + \tilde{\mathbf{G}}_m(\tilde{\theta}_v, \mathbf{q}_m)$$

$$= \mathbf{J}_{fbm}^T(\mathbf{q}_m)\begin{bmatrix} \tilde{\mathbf{R}}_v^T(\tilde{\theta}_v) & \mathbf{0} \\ \mathbf{0} & \tilde{\mathbf{R}}_v^T(\tilde{\theta}_v) \end{bmatrix}\tilde{\mathbf{F}}_{edes} + \tilde{\mathbf{G}}_m(\tilde{\theta}_v, \mathbf{q}_m) \quad (5)$$

where $\mathbf{F}_{edes}$ is a 6 element column vector of virtual forces and torques reflected to the end-effector:

$$\tilde{\mathbf{F}}_{edes} = [\mathbf{K}_p]\{\mathbf{x}_{edes} - \tilde{\mathbf{x}}_e(\tilde{\mathbf{r}}_v, \tilde{\theta}_v, \mathbf{q}_m)\}$$

$$+ [\mathbf{K}_d]\{\dot{\mathbf{x}}_{edes} - \tilde{\mathbf{M}}\tilde{\mathbf{M}}\mathbf{J}(\tilde{\theta}_v, \mathbf{q}_m)\,\dot{\mathbf{q}}\} \quad (6)$$

The n element column vector $\mathbf{G}_m$ compensates for manipulator gravity loads, and the terms $\mathbf{x}_{edes}$ and $\dot{\mathbf{x}}_{edes}$ represent the desired endpoint position and velocity, respectively. The symbol " ~ " denotes terms known only approximately due to limited vehicle sensing, see Figure 2.

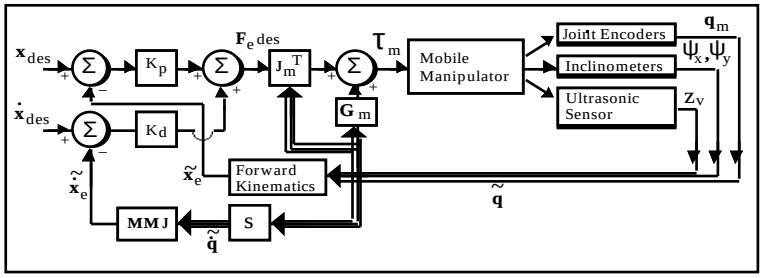

Fig. 2. MMJT Control Block Diagram.

c. Mobile Manipulator Resolved Rate Control

A second mobile manipulator control algorithm was developed based on the resolved rate algorithm [13]. The latter algorithm is not directly applicable due to the non-square, and therefore non-invertible, mobile manipulator jacobian matrix. Instead, relying on the MMJ sub-jacobian matrices presented above, a mobile manipulator resolved rate algorithm (MMRR) was derived, which combines with a conventional proportional derivative joint controller and a gravity compensation torque to eliminate steady state gravitational offsets, as follows [12]:

$$\tau_m = [\mathbf{K}_p]\,\tilde{\mathbf{J}}_m^{-1}\{\mathbf{x}_{edes} - \tilde{\mathbf{x}}_e\} + [\mathbf{K}_d]\{\dot{\tilde{\mathbf{q}}}_{mdes} - \dot{\tilde{\mathbf{q}}}_m\} + \tilde{\mathbf{G}}_m \quad (7)$$

where

$$\tilde{\dot{\mathbf{q}}}_{mdes} = \mathbf{J}_{fbm}^{-1} \begin{bmatrix} \tilde{\mathbf{R}}_v^T & \mathbf{0} \\ \mathbf{0} & \tilde{\mathbf{R}}_v^T \end{bmatrix} \{\dot{\mathbf{x}}_{edes} - \tilde{\dot{\mathbf{x}}}_v\} + \begin{bmatrix} [\tilde{\mathbf{r}}_{Ve}]\times \tilde{\mathbf{R}}_v^T \\ \mathbf{0} \end{bmatrix} \tilde{\omega}_v \quad (8)$$

III. THE EXPERIMENTAL SYSTEM

The MMJT control algorithms were implemented experimentally on a PUMA 260 manipulator mounted on the MIT Vehicle Emulation System I (VES I) in the MIT Mobile Manipulator Laboratory, see Figure 3. The VES, a six DOF hydraulically actuated Stewart platform operating under admittance control, can experimentally emulate a wide variety of nonlinear compliant vehicles [14].

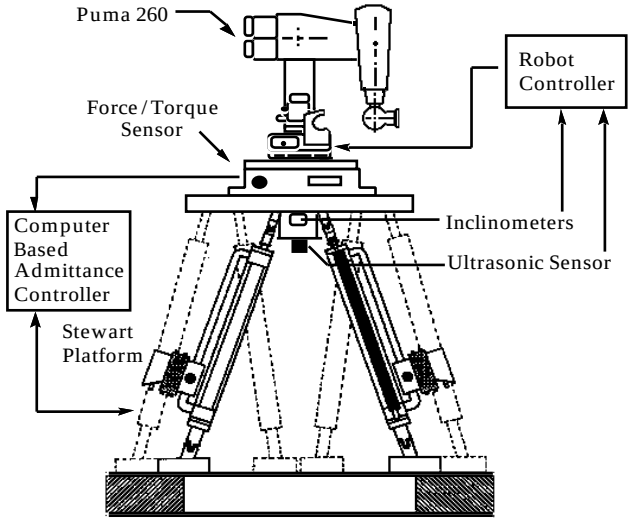

Fig. 3. The Experimental System Hardware.

A six DOF force and torque sensor is mounted on top of the platform and underneath the PUMA. It measures the dynamic interactions between the manipulator and its vehicle, the Stewart platform. Based on these forces and torques the admittance controller solves a dynamic model of the emulated vehicle to determine its corresponding motion, and then commands the Stewart mechanism to track that motion.

Vehicle sensors were limited to those readily applicable in unstructured field environments: an ultrasonic sensor measuring vertical motion, and inclinometers measuring pitch and roll angles, see Figure 2. These sensors are simple, low in cost, and readily available, but are noisy, and have considerable lag and time delay. One of the questions to be investigated was

whether the control algorithm would tolerate such non-ideal characteristics of vehicle sensors, in addition to the lack of sensing in certain directions.

IV. EXPERIMENTAL MM CONTROL ALGORITHM PERFORMANCE

The VES admittance model was chosen so that the PUMA/VES mobile manipulator represented a scaled down version of a prototype system developed in Reference [12]. Figure 4 shows the measured manipulator/vehicle dynamic interaction forces during a 5 second, approximately 0.5 meter, straight line planar manipulator upward move. Clearly, as shown in Figure 5, the dynamic interaction leads to large vehicle motion. Also, the sensor signals show significant inaccuracies and time delays.

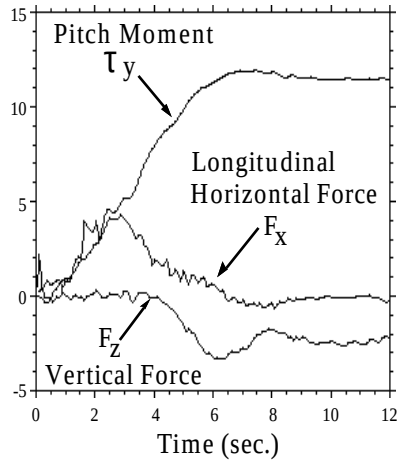

Fig. 4. Manipulator/Vehicle Interaction Forces.

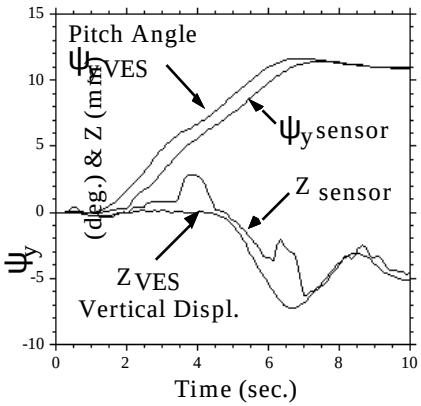

Fig. 5. Performance of Vehicle Sensors.

Figure 6 shows the manipulator endpoint performance for the above experiment using PD joint control as well as both MMJT and MMRR control [12,15]. In contrast to the inadequate conventional controller, the MMJT and the MMRR controllers both compensate for vehicle

dynamic motions with much smaller dynamic endpoint errors while relying on only low-cost, readily available, but relatively slow and inaccurate vehicle motion sensors.

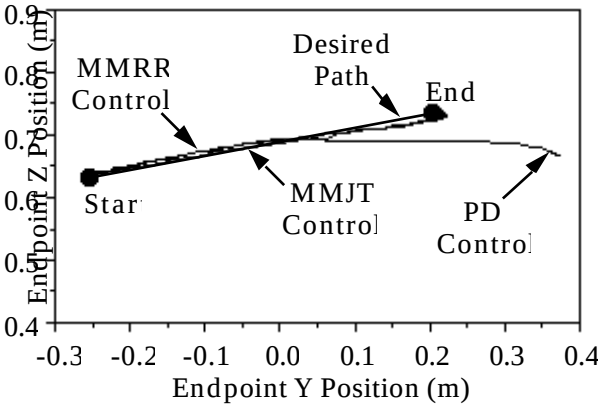

Fig. 6. MMJT, MMRR and PD Endpoint Motion.

Figure 7 shows similar results during a 5 second, approximately 0.5 meter, straight line planar downward move. This figure shows the endpoint errors for the MMRR, MMJT, and PD controllers. The MMRR controller has a maximum endpoint error of 20 mm and a steady state endpoint error of 2.5 mm. The MMJT controller shows a maximum error of 23 mm and a steady state error of 3 mm. The PD controller has the largest maximum and steady state errors which are 139 mm and 130 mm, respectively.

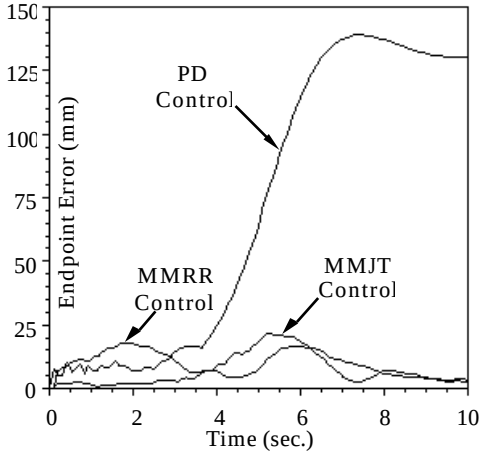

Fig. 7. MMJT, MMRR and PD Endpoint Errors.

The performance of the MMJT and MMRR algorithms is similar in terms of the size of their maximum and steady state errors. Note that both controllers exhibit larger endpoint errors at the end of the downward trajectory as they "overshoot" the target endpoint. However, during the line motion, the MMJT controller shows significantly less endpoint tracking error

than the MMRR controller. Since the desired task motion is generally defined in world-space, the desired end-effector trajectories tend to be much smoother than the corresponding joint trajectories. The MMRR controller is sensitive to swift joint configuration changes during the manipulator move, and as a result tends to have a second peak in its tracking error.

The overshoot at the end of the manipulator trajectory, noted for both the MMJT and the MMRR controller, is caused by lags in the control feedback loop. At this time vehicle motion is largest and the system is most sensitive to lags due, particularly, to vehicle sensor limitations. Figure 8 shows the effect of vehicle sensor time delay on the manipulator's experimental ability to track its 0.5 meter endpoint upward trajectory in 2.0 seconds under MMJT control. The results suggest that even for low performance manipulator systems the effects of time delays can be seen and hence this issue should be considered during the design process. Similarly, Figure 9 shows the effect of sensor errors introduced into the vehicle orientation measurements. This figure of experimental endpoint errors under MMJT control clearly shows the direct correlation between sensor accuracy and manipulator endpoint errors.

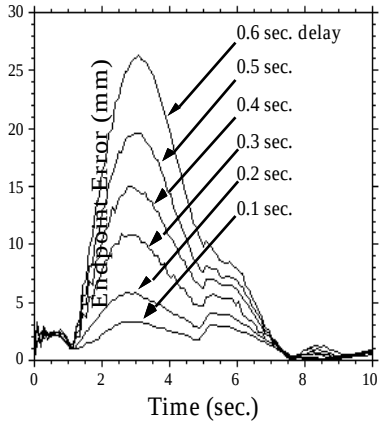

Fig. 8. Experimental MM Endpoint Error vs. Vehicle Sensor Time Delay.

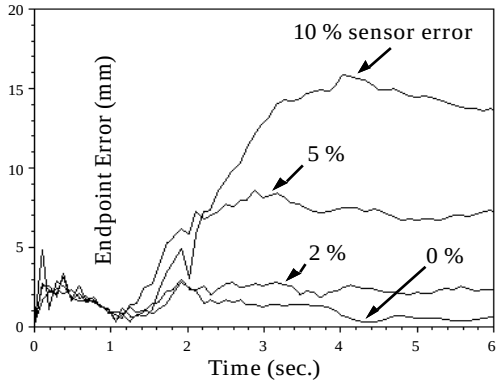

Fig. 9. Experimental MM Endpoint Error vs. % Inclinometer Error.

V. CONCLUSION

Experimental results have shown that dynamic interactions between a mobile manipulator and its vehicle can lead to large endpoint errors when a conventional fixed-base controller is used. The Mobile Manipulator Jacobian Transpose (MMJT) and the Mobile Manipulator Resolved Rate (MMRR) control algorithms, which account for dynamic vehicle motions, were both shown to provide good, stable nonlinear large motion control, while using only limited vehicle sensory data, such as would be practically available in highly unstructured field environments. The MMJT algorithm was seen to be slightly superior to the MMRR algorithm. Filter lags, sensor lags, time delays and accuracy errors were shown to be directly correlated with experimental endpoint errors, and should be considered specifically during the design process of mobile manipulator systems.

VI. ACKNOWLEDGEMENT

The support of this work by DARPA (Martin Marietta Subcontract No. 19X-5570C) and NASA (Langley Research Center, Automation Branch) under Grant NAG-1-801 is acknowledged.

VII. REFERENCES

[1] Anderson, M.R., "Ecological Robots," *The MIT Technology Review*, January, 1992, pp. 22-23.

[2] Khatib, O, "A Unified Approach for Motion and Force Control of Robot Manipulators: The Operational Space Formulation," *IEEE J. Robotics & Automation*, Vol. RA-3, No. 1, Feb. 1987, pp. 43-53.

[3] Wiens, G.J., "Effects of Dynamic Coupling in Mobile Robotic Systems," *Proceedings of the SME Robotics Research World Conference*, Gaithersburg, MD, Vol. 3, May 7-11, 1989, pp.43-57.

[4] Murphy, S.H., Wen, J.T.-Y., and Saridis, G.N., "Simulation of Cooperating Robot Manipulators on a Mobile Platform," *IEEE Trans. Rob. and Automation*, Vol. 7, No. 4, Aug. 1991, pp. 468-478.

[5] Dubowsky, S., Gu, P.-Y., and Deck J.F., "The Dynamic Analysis of Flexibility in Mobile Robotic Manipulator Systems," *Proc. of the Eighth World Congress on the Theory of Machines and Mechanisms*, Prague, Czechoslovakia, August 26-31, 1991.

[6] Dubowsky, S., and Tanner, A.B., "A Study of the Dynamics and Control of Mobile Manipulators Subjected to Vehicle Disturbances," *Proceedings of the Fourth International Symposium of Robotics Research*, Santa Cruz, CA, August 9-14, 1987.

[7] Dubowsky, S., and Vance, E.E., "Planning Mobile Manipulator Motions Considering Vehicle Dynamic Stability Constraints," *Proc. IEEE International Conference on Robotics and Automation*, Vol. 3, Scottsdale, AZ, May 14-19, 1989, pp. 1271-1276.

[8] Chiang, W.W., "End-Point Position Control of a Flexible Manipulator with a Quick Wrist," *Ph.D. Thesis, Dept. Aeronautics & Astronautics, Stanford University*, Stanford, CA, April 1985.

[9] Sharon, A., "The Macro/Micro Manipulator: An Improved Architecture for Robot Control," *Ph.D. Thesis, Department of Mechanical Engineering, MIT*, Cambridge, MA, September 1988.

[10] West, H., Hootsmans, N., Dubowsky, S., Stelman, N., "Experimental Simulation of Manipulator Base Compliance," *Proceedings of the First International Symposium on Experimental Robotics*, Montreal, Canada, June 19-21, 1989.

[11] Hootsmans, N.A.M., and Dubowsky, S., "Large Motion Control of Mobile Manipulators Including Vehicle Suspension Characteristics," *Proceedings of the IEEE International Conference Robotics and Automation*, April 7-12, 1991 pp. 2336-2341.

[12] Hootsmans, N.A.M., "The Motion Control of Manipulators on Mobile Vehicles," *Sc.D. Thesis, Department of Mechanical Engineering, MIT*, Cambridge, MA, January, 1992.

[13] Whitney, D.E., "Resolved Motion Rate Control of Manipulators and Human Prostheses," *IEEE Transactions on Man-Machine Systems*, Vol. MMS-10, No.2, June 1969, pp. 47-53.

[14] Dubowsky, S., Paul, I., and West, H., "An Analytical and Experimental Program to Develop Control Algorithms for Mobile Manipulators," *Proc. 7th CISM-IFToMM Symposium on Theory and Practice of Robots and Manipulators*, Sept., 1988, Udine, Italy.

[15] Mo, P.Z., "Experimental Performance of a Mobile Manipulator Resolved Rate Algorithm for Large Motion Endpoint Control," *Sc.B. Thesis, Department of Mechanical Engineering, MIT*, Cambridge, MA, March, 1992.